Large Strain Work Hardening of Aluminum Alloys and the Effect of Mg in Solid Solution

ØYVIND RYEN, HANS IVAR LAUKLI, BJØRN HOLMEDAL, and ERIK NES

The work-hardening behavior of a range of aluminum-magnesium alloys, from 0.5 to 4.55 wt pct Mg, is followed up to large strains using compression testing and cold rolling. At large strains, stage IV, an unexpectedly low work-hardening rate of high-Mg alloys is observed, and the work-hardening rate in stage IV is almost unaffected by the Mg content. A model for work hardening is applied and discussed in relation to the experimental observations. Based on microstructural observations of the cold-rolled materials, the low work-hardening rate of high-Mg alloys is ascribed to a different storage pattern of dislocations caused by an increased amount of shear bands and a higher dislocation density inside subgrains.

I. INTRODUCTION

MATERIAL properties at large strains ($\varepsilon > 0.7$) are of significant importance for a number of applications, such as in cold rolling of sheets and the subsequent forming or annealing operations. Studies of the material behavior through all stages of work hardening are therefore of interest. When polycrystals are considered, it is common to distinguish between stages II, III, and IV (reviewed by Rollett and Kocks[1]). Stage II has, under ideal conditions, a high and constant work-hardening rate of the order $G/200$, where G is the shear modulus. The stage is associated with an accumulation of dislocations, but eventually dynamic recovery reactions start taking place. This leads us into stage III, where the hardening rate decreases and the stress–strain curve becomes parabolic. In most commercial alloys, distinguishing stage II from III is difficult because the distribution of grain sizes and the presence of particles contribute to a parabolic hardening also in stage II.

A stage of sustained hardening following stage III is commonly described in treatments of large strain work hardening. One of the first well-documented observations of a stage IV is the oft-cited work by Langford and Cohen,[2] where the strength of a drawn iron wire was seen to increase linearly up to strains of $\varepsilon = 7$. Torsion tests of aluminum and copper also reveal a stage IV,[3,4] and so does ECAP processing.[5] Perhaps the most common experimental method used to obtain stage IV is rolling (see Gil Sevillano[6] for references). The stage IV work-hardening rate is often found to be of the order $2 \cdot 10^{-4}\ G$, considerably lower than the rate of stage II. While the behavior of AlMg alloys in stage II and III is well described in the literature (*e.g.,* in the early work by Sherby *et al.*[7]), the effect on stage IV of adding Mg to the alloy is not clear.

Cold rolling followed by tensile testing is a well-established method for obtaining large strain data. One problem that inevitably arises when stage IV is discussed is that there exists no method by which a material can be tested continuously or without some shape change, path change, texture change, or friction. All these aspects must be kept in mind and the results should be treated carefully.

A number of models for the work-hardening behavior of metals have been proposed during the past 30 years. One of the earliest, and perhaps the most widely known, is the model initially presented by Kocks[8] and further developed in collaboration with Mecking (for a recent update see Reference 9). This modeling concept, commonly referred to as the MTS model (mechanical threshold strength[10]), is a one-parameter description with an overall dislocation density as the only internal variable. The model predicts a Voce behavior of the stress–strain curve (*i.e.,* a stress saturation), but in later refinements by Rollett *et al.*,[11] a dislocation debris approach is included to account for the stage IV hardening. A recent re-examination of the debris model has been presented by Holmedal *et al.*[12] A different modeling concept includes a more precisely specified refinement of the cell/subgrain structure.[13,14,15] Experimental support for this can be found in the works of Castro-Fernandez *et al.*[16] and Langford and Cohen.[2] On the other hand, Argon and Haasen[17] suggested that the hardening is caused by misfit stresses in the cells, giving rise to the rate-independent hardening in stage IV. The topic is still a matter of discussion.

In this paper a work-hardening model developed by Nes *et al.*[18–21] will be applied. The work-hardening behavior of a range of AlMg alloys will be presented and discussed from both experimental and modeling points of view. The model has shown some discrepancies with respect to the experiments at large strain deformation at room temperature, and an effort is made here to make this aspect of work hardening somewhat clearer.

II. EXPERIMENTAL PROCEDURE

Five alloys of commercial purity grades, spanning an Mg concentration from 0 to 4.55 wt pct, were investigated in this work (Table I). All of them had a coarse, equiaxed grain structure and a nearly random texture. AA1050 is a commercially pure alloy with small amounts of Fe and Si. Three AlMgX alloys, where X = 0.5, 1, and 3 wt pct Mg, were designed to be as close as possible to AA1050 with respect to the Fe and Si content. The AA1050 alloy could therefore be regarded as an Mg-free reference material for the AlMgX alloys. In addition, the high-Mg alloy AA5182 was investigated. All the materials were delivered

ØYVIND RYEN, Project Engineer, is with Reinertsen Engineering AS. HANS IVAR LAUKLI, Research Scientist, is with Hydro Aluminum, Sunndalsøra, Norway. BJØRN HOLMEDAL, Research Scientist, and ERIK NES, Professor, are with the Norwegian University of Science and Technology, Troudheim, Norway. Contact e-mail: erik.nes@material.ntnu.no

Manuscript submitted August 12, 2005.

Table I. Details of Alloys

Alloy	Mg (Wt Pct/At. Pct)	Mn (Wt Pct)	Si (Wt Pct)	Fe (Wt Pct)	Al (Wt Pct)	Initial Grain Size (μm)
AA1050	0.002/0.002	0.003	0.09	0.27	bal. (99.6)	117
AlMg0.5	0.48/0.53	0.008	0.04	0.18	bal.	86
AlMg1	1.01/1.12	0.008	0.06	0.19	bal.	79
AlMg3	2.93/3.24	0.01	0.06	0.20	bal.	68
AA5182*	4.55/5.02	0.27	0.11	0.21	bal.	50

*Supplied by Pechiney, now Alcan Voreppe. Other alloys supplied by Hydro Aluminum Sunndal.

in the DC-cast condition, except for AA5182, which was homogenized and hot rolled into a 25-mm transfer slab gauge. After casting, the AA1050 and AlMgX alloys were given an industrial homogenization procedure in an air-circulating furnace (6 hours at 550 °C, slowly heated and cooled).

The AA1050 and AlMgX alloys were tested in their O-temper conditions by uniaxial compression of cylindrical specimens with a diameter/height ratio of 10/15 mm and an initial strain rate of 0.01 s^{-1}. This was carried out in collaboration with S. Zajac at the Swedish Institute for Metals Research[22] and B. Rønning at Hydro Aluminum Sunndal.[23] Boron nitride powder was used as a lubricant to eliminate friction between specimens and tools during compression, and only a minimal amount of barreling was detected within the strain range tested. The AA5182 alloy was tested in uniaxial tension of flat specimens (cross-section 25 × 7.7 mm^2, length 80 mm, strain rate $6 \cdot 10^{-3}$ s^{-1}) in collaboration with Hydro Aluminum Deutschland.[24]

Cold rolling was carried out in a laboratory mill at a relatively low strain rate, typically 1 s^{-1}, where the temperature was kept below 40 °C. The strain obtained during rolling was calculated from the initial and final thickness, t_0 and t. Throughout this paper the equivalent von Mises strain (ε_{vM}) is used, defined for rolling as:[25]

$$\varepsilon_{vM} = \frac{2}{\sqrt{3}} \ln \frac{t_0}{t} \qquad [1]$$

where $\ln(t_0/t)$ = the logarithmic principal strain (ε). Tensile specimens were taken from the rolled sheets with the tensile axis parallel to the rolling direction. For rolling strains of 0.5 and 1, round specimens 6 mm in diameter and 30 mm in gauge length were used, whereas for strains of 2 (thickness 3.4 mm) and 3 (thickness 1.2 mm), the final sheet thickness defined the specimen thickness (width 6 mm, gauge length 30 mm). The global texture evolution during cold rolling was measured by X-ray diffraction in the sheet normal plane in the middle of the sheet. X-ray diffraction of 5182 was performed at Katholieke Universiteit Leuven.[26] Taylor factors were calculated by means of the full constraints (FC) Taylor model implementation in the MTM-FHM software.[27] Microstructural investigations were performed in the longitudinal transverse section. Light optical microscopy, scanning electron microscopy (SEM), with equipment for electron back-scatter diffraction (EBSD), and transmission electron microscopy (TEM) were used to study the microstructural evolution during cold rolling.

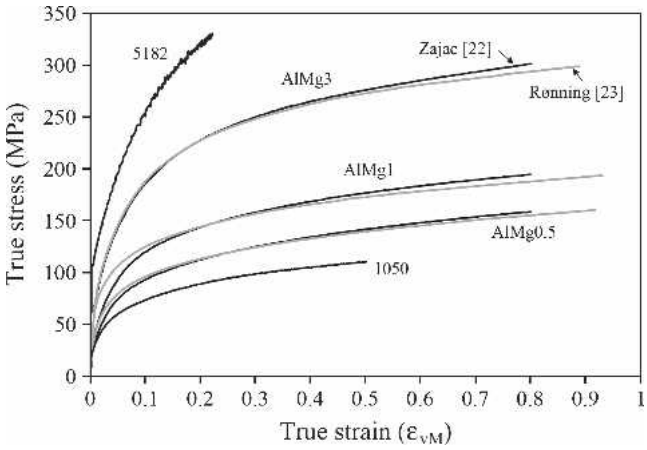

Fig. 1—Stress–strain curves from uniaxial compression of AA1050 and AlMgX and uniaxial tension of AA5182.[24] Note that there are two sets of experiments for the AlMgX alloys.[22,23]

Throughout this paper the work-hardening rate is defined in accordance with the common terminology:

$$\theta = \frac{d\tau}{d\gamma} \qquad [2]$$

where τ and γ = the resolved shear stress and strain, respectively. The hardening rate obtained from the stress–strain curves of polycrystalline samples can therefore be written as:

$$\frac{d\sigma}{d\varepsilon} = M^2\theta \qquad [3]$$

where M = the Taylor factor calculated from the measured texture.

III. RESULTS AND DISCUSSION

A. *Mechanical Properties and Work Hardening*

Results from uniaxial compression tests of the AlMgX alloys and AA1050 are shown in Figure 1. These data are almost identical to the tensile data from the same alloys but provide continuous curves up to a strain of $\varepsilon_{vM} = 0.7$ to 0.8. The stress–strain curve from uniaxial tension of AA5182 is shown in the same diagram. With increasing Mg content, the yield strength and the initial work-hardening rate are seen to increase, in agreement with several other observations.[7,28] A more detailed study of the solute effects on

strength at low strains is reported in an accompaning work by Ryen *et al.*[29] As the strain increases, the hardening rate decreases (stage III) before it approaches a linear stage of work hardening recognized as stage IV. The work hardening rate ($d\sigma/d\varepsilon$) as a function of the Mg content at two different strain levels in the compression tests, $\varepsilon_{vM} = 0.45$ and 0.7, is plotted in Figure 2. The results of Zajac[22] and Rønning[23] were slightly scattered, so an average is taken between these. It is seen that the hardening rate decreases with strain but depends on the presence of Mg throughout the compression test. The *reduced* work hardening rate, defined as:

$$\frac{\theta}{G} = \frac{1}{M^2 G} \cdot \frac{d\sigma}{d\varepsilon} \qquad [4]$$

is in the range 2 to $3 \cdot 10^{-4}$ for $\varepsilon_{vM} = 0.7$, assuming a Taylor factor of $M = 3.07$ (see Section III–B) and a shear modulus $G = 25.5$ GPa. This work-hardening rate is not far from what is frequently reported in the literature[1,6]—*i.e.,* for high-purity aluminum, $2.7 \cdot 10^{-4}$ at room temperature and $5.4 \cdot 10^{-4}$ at 77 K; the corresponding data for copper are $5.5 \cdot 10^{-4}$ and $8.3 \cdot 10^{-4}$.

In Figure 3 both the initial yield stress ($R_{p0.2}$) and the true uniform stress (σ_u at maximum load) from tensile tests of the cold-rolled materials are plotted as a function of the rolling strain, thereby extending the stress–strain curves in Figure 1 to large strains. The curves are seen to be practically linear, at least for strains above $\varepsilon_{vM} = 1$, and clearly the alloys reveal a stage IV of work hardening, even though some of the curves are slightly curved downward, an aspect frequently found to be associated with stage IV hardening.[6,20] It is noted that the $R_{p0.2}$ values are significantly lower than the plotted σ_u, probably because of static recovery after rolling. A consequence of such a recovery effect is additional deformation beyond the yield point as a necessary transition to restore stage IV in the material. Even σ_u might underestimate the true stage IV flow stress, because during this transition the Considère criteria for the onset of necking are met prior to reaching σ_u. The small discrepancy between the compression data and rolling + tension data around $\varepsilon_{vM} = 0.6$ may relate to an increased friction in compression. On the other hand, it might also be an effect of the moderate change in strain path and stress state when changing from rolling to tension. However, the best data to represent the stage IV flow stress beyond the compression curves become these σ_u values derived from tensile testing, and these data will be used in the following discussion and modeling of stage IV.

The first data point in Figure 3 that is clearly in stage IV is at $\varepsilon_{vM} = 1.15$. A straight line can be drawn from this point and beyond, giving a work-hardening rate in the large strain range that is plotted in Figure 2. This strain range is considered as a true stage IV, as the interpolated stress–strain curve is approximately linear. As seen in Figure 2, the work-hardening rate obtained by cold rolling depends much less on the Mg content than what follows from the compression data at $\varepsilon_{vM} < 1$. This is a striking result, as a number of works may lead to a general conception that the hardening rate scales with the flow stress. For example, in a work on copper deformed in torsion over a large range of temperatures,[3,6] the hardening rate in stage IV θ_{IV} followed the flow stress at the onset of stage IV τ_{IV}, as in:

$$\theta_{IV} = a \cdot \tau_{IV} \qquad [5]$$

where a = a constant. Tensile testing of AlMg alloys shows that an increase in solute content has the same effect as a reduction in temperature on the work hardening in stage II and III.[7] Accordingly, it might be reasonable to anticipate a behavior like Eq. [5] also by increasing the Mg content. However, as seen in Figure 4, where the ratio $M^2\theta/\sigma$ is plotted as a function of Mg content, a is not constant for the present alloys. The reason for this decay in the ratio between work-hardening rate and flow stress as the Mg content is increased is sought in the texture and microstructure of the cold-rolled material.

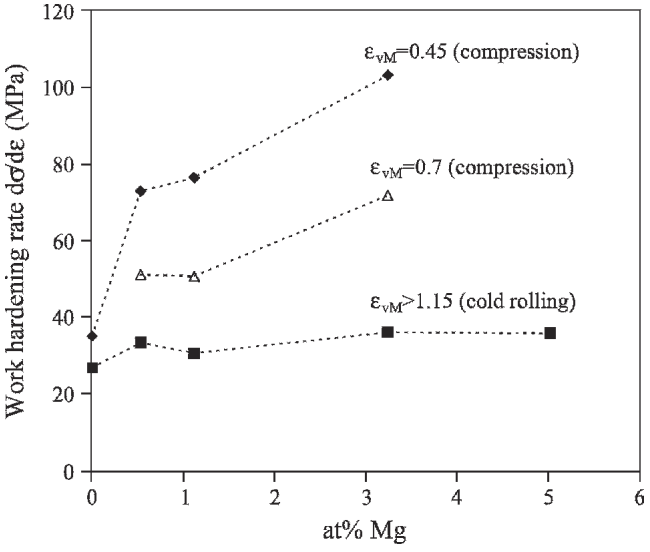

Fig. 2—The work-hardening rate as defined by Eq. [3] at three strain levels, $\varepsilon_{vM} = 0.45$ and 0.7 from compression tests and $\varepsilon_{vM} > 1.15$ from rolling + tension tests.

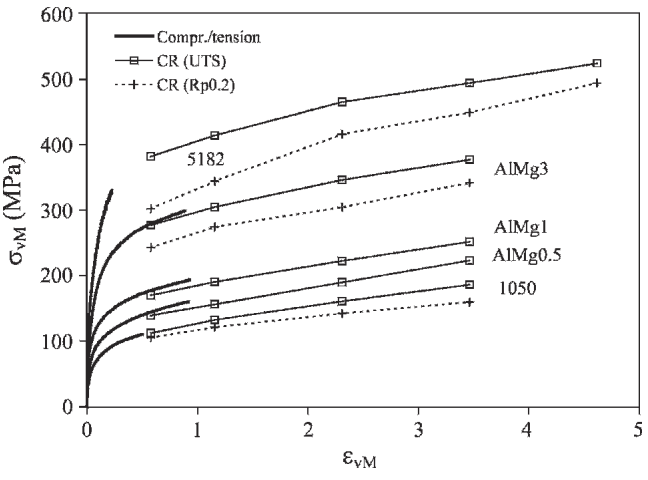

Fig. 3—Results from tensile testing of cold rolled materials, plotted along with the compression[23] and tension curves from Figure 1. The true ultimate stress is plotted for all alloys. In addition, the $R_{p0.2}$ values are plotted for AA1050, AlMg3, and AA5182.

B. *Texture and Microstructure*

The rolling texture of the investigated alloys is dominated by a typical β-fiber as shown in Figure 5, which includes the components copper = $\{112\}\langle 111\rangle$, S = $\{123\}\langle 634\rangle$, and brass = $\{011\}\langle 211\rangle$ (arrows in the figure). For a general introduction to this kind of texture representation, see Randle and Engler.[30] The intensity of the β-fiber increases with rolling reduction, but only slightly at $\varepsilon_{vM} > 2$. Some differences with solute are also seen (Figure 5) as the brass component becomes stronger when the Mg content increases from 0 to 3 pct, an effect explained by shear banding[31,32] and by the influence of the increased strength and work hardening on short-range grain interactions.[33] A further increase in Mg content (AA5182) gives a density of shear bands so high that the texture becomes randomized. However, the texture differences are so small that the variations in Taylor factor calculated from the measured textures have a negligible effect on the work hardening in stage IV. Assuming an average Taylor factor of $M = 3.07$ for all alloys and rolling strains gives an error of less than 5 pct from the results obtained using the MTM-FHM software[27] in calculating the Taylor factors on the basis of the measured textures.

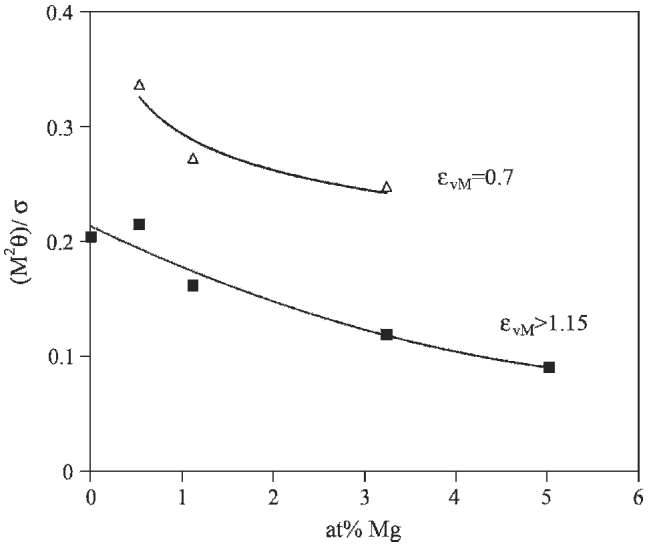

Fig. 4—The ratio between work-hardening rate and flow stress $M^2\theta/\sigma$ plotted as a function of Mg content. The upper curve is from compression tests, using the flow stress and hardening rate at $\varepsilon_{vM} = 0.7$. The lower curve is from rolling + tension experiments, using the flow stress at $\varepsilon_{vM} = 1.15$ and the average hardening rate from $\varepsilon_{vM} = 1.15$ and up to the maximum strain that is tested.

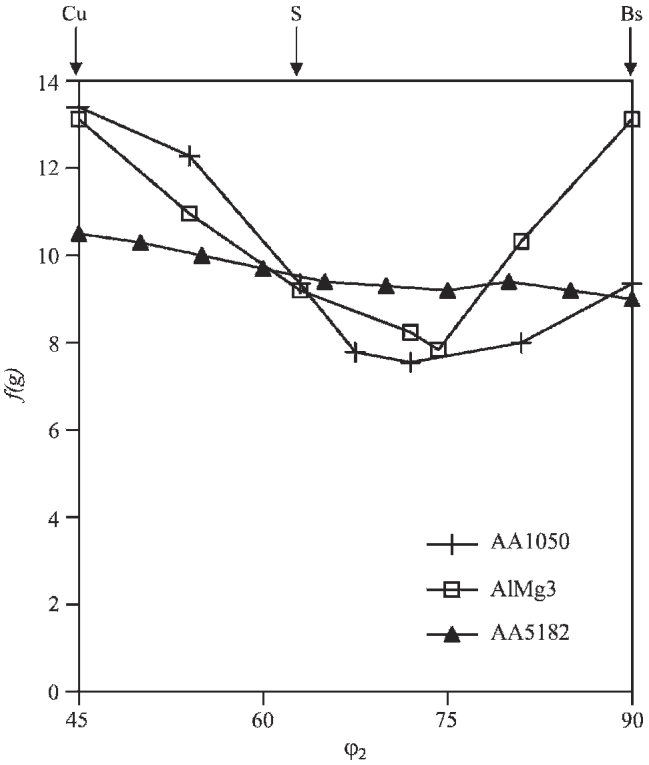

Fig. 5—β-fiber density plot of AA1050, AlMg3, and AA5182 cold rolled to $\varepsilon_{vM} = 3.45$. The texture components copper (Cu), S, and brass (Bs) are indicated by arrows.

As indicated by the texture results, but also known as a frequently occurring phenomenon during rolling of AlMg alloys,[34] shear bands are formed in these alloys. Figure 6 shows the microstructure of AlMg1 and AA5182 after cold rolling to $\varepsilon_{vM} = 3.45$. Shear bands are formed in both alloys, but the amount of bands is much higher in the high-Mg alloy AA5182 than in AlMg1. A quantification of the banding has not been attempted in this work, but a qualitative characterization is performed. The dotted line in Figure 7 illustrates that the critical cold-rolling strain necessary for the formation of shear bands decreases with increasing concentration of Mg, which is in agreement with the observations of Inagaki and Kohara.[34]

Material volumes within the shear bands are subjected to extensive dynamic recovery,[35] perhaps due to a local temperature increase resulting from the intense shear deformation. A coarser subgrain structure within shear bands in cold-rolled ferritic steels has been reported by Roven and Nes.[36] Harren *et al.*[37] found that lattice reorientations within shear bands could produce geometrically softened channels that concentrate the strain. The shear bands may therefore accommodate large strains in hard oriented grains,[38] with a corresponding reduction of the overall work hardening compared to that expected. All in all, it is reasonable to believe that the formation of shear bands may result in local work softening of the material. The relatively low work-hardening rate in stage IV of AlMg alloys occurs along with an increasing amount of shear bands with Mg content. This is a plausible explanation for the low rate of work hardening in stage IV of the AlMg alloys.

Another significant effect on the microstructural evolution by adding Mg to the alloy is seen in the spatial distribution of dislocations. In high-Mg alloys, the dislocation density inside the subgrains after cold rolling is much higher than, for instance, in AA1050 (Figure 8). At the same time, the subgrain size is observed to become somewhat smaller when the Mg content is increased.

C. *Modeling of Work Hardening*

The model applied here for the work-hardening and substructure evolution of fcc metals has been developed by Nes and Marthinsen, *et al*. This model provides the flow stress

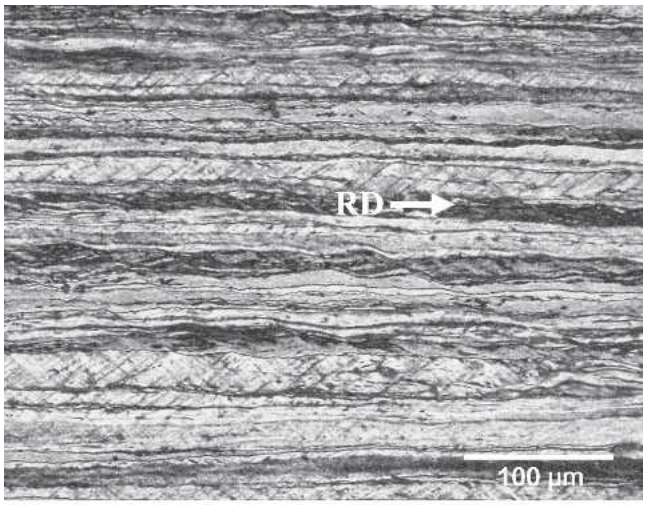

(*a*)

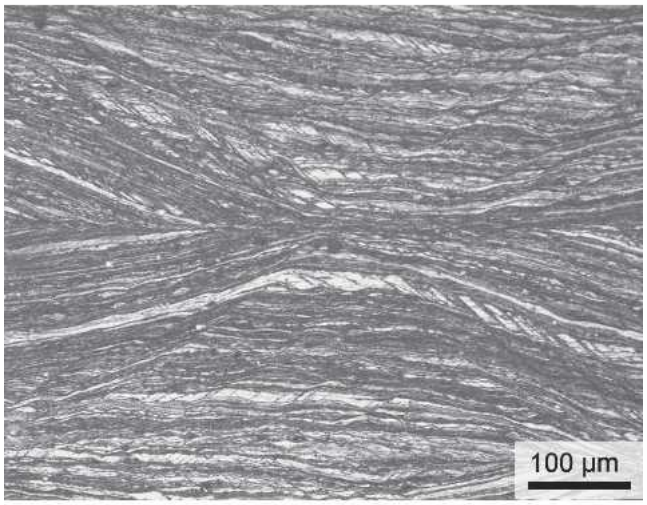

(*b*)

Fig. 6—Optical micrographs of (*a*) AlMg1 and (*b*) AA5182 after cold rolling to a strain of $\varepsilon_{vM} = 3.45$.

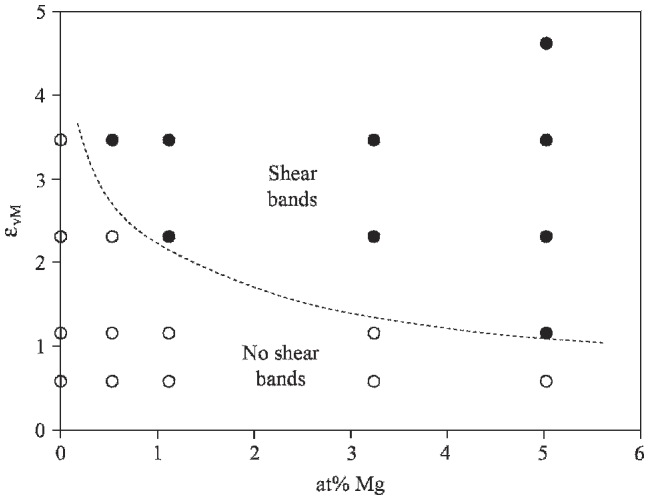

Fig. 7—The formation of macroscopic shear bands as a function of cold-rolling strain and at. pct Mg in the alloy. Full circles and open circles represent shear band formation and no shear band formation, respectively.

and substructural parameters as a function of the applied deformation history. A comprehensive description of the model is given in several papers,[18–21] so only a few aspects of specific relevance for the current work are presented here.

The model relies on a multiparameter description of the microstructure evolution, which at large strains is characterized by subgrains of size δ, subboundaries of misorientation φ, and a dislocation density inside the subgrains ρ_i. The flow stress at a constant microstructure and large grains is given by:

$$\tau = \tau_t + \tau_p + \alpha_1 Gb\sqrt{\rho_i} + \alpha_2 Gb\delta^{-1} \qquad [6]$$

where τ_t and τ_p = the thermal component and the particle contribution respectively and α_1 and α_2 = constants. Multiplying τ with the Taylor factor, which can be obtained from texture measurements or modeling, gives the global stress σ. Differential equations for the evolution of each of the microstructural parameters must be solved to predict the flow stress as a function of the strain γ. Magnesium in solid solution will affect all aspects of work hardening—*i.e.,* the thermal component of the flow stress, the athermal storage rate of dislocations, and their dynamic recovery rate. The major effect, however, on the work hardening in stages II and III relates to the retardation of dynamic recovery (see Marthinsen and Nes[19]). The solute effect on the thermal component is in this context relatively small (see the work on dynamic strain aging by Holmedal *et al.*[18]). Of main concern here, however, is stage IV work hardening, which according to the stress strain curves in Figure 2 appears nearly solute-invariant.

Storage occurs in three different ways: in a Frank network, by increasing the misorientation of already existing boundaries, or by creating new boundaries. According to the model, the storage rate related to the latter mechanism results in a refinement of the subgrain size:

$$\frac{d\delta^-}{d\gamma} = -\frac{2SC^2\delta^2\rho_i L}{\kappa_0\varphi} \qquad [7]$$

Here $L = C\sqrt{\rho}$ is a statistical slip length (*i.e.,* the distance a mobile dislocation travels from the source until becoming stored in the substructure), C = a constant, and ρ = the total dislocation density (*i.e.,* the sum of the dislocations stored in the Frank network within the cells and those stored in the cell/subgrain boundaries; in stages III and IV, $\rho = \rho_i + \kappa_0\varphi/\delta$, where κ_0 is a geometrical shape factor of order 3. The constant C can be determined experimentally from stress–strain curves of single crystals or coarse-grained metals, where this constant is related to the work-hardening rate in stage II, θ_{II}, through $C = \alpha_1 G/\theta_{II}$. An empirical expression is used for the misorientation, saying that φ increases with strain to a saturation level, φ_{IV}, of 3 deg in the early stage IV, and S is a statistical sub-boundary storage parameter. The storage parameter S is under stage II conditions, where microstructural scaling or similitude applies, defined as ($S \equiv S_{sc}$); in terms of the scaling parameters, subsequent hardening is caused solely

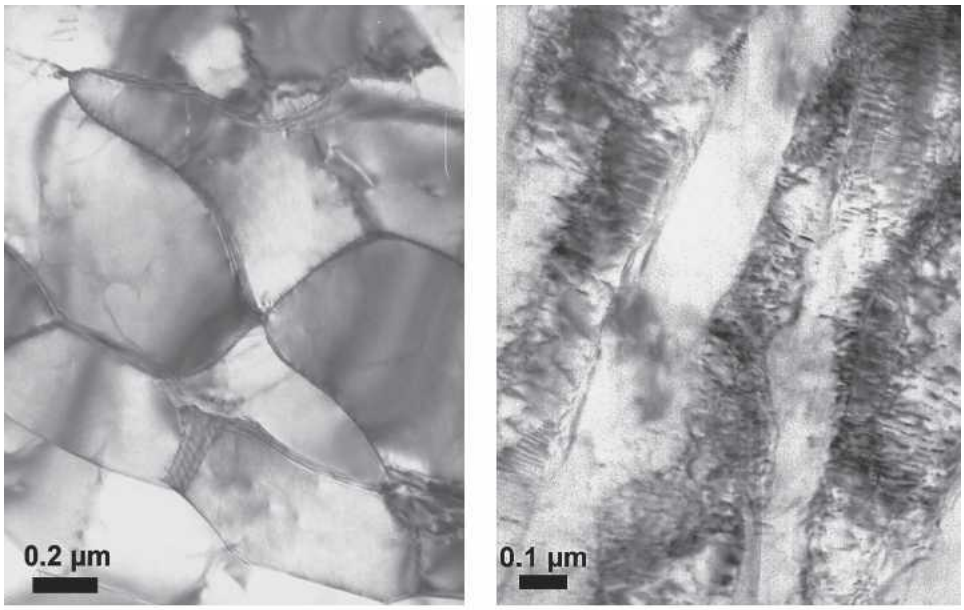

Fig. 8—TEM micrographs showing a difference in the spatial distribution of dislocations when the Mg content is increased from zero in AA1050 (*a*) to 3 pct in AlMg3 (*b*). Both alloys are cold rolled to $\varepsilon_{vM} = 2.3$.

by a refinement of the subgrain structure. The stage IV work hardening rate, θ_{IV}, is then approximately constant, given by:

$$\theta_{IV} = \alpha_2 Gb \frac{2\rho_i C S_{IV}}{\kappa_0 \varphi_{IV} \sqrt{\rho}} \quad [8]$$

At present, shear banding is not included in the model. An indirect method to implement shear bands in the model can be to ascribe the phenomenon to a different storage mode. In the competition between the mechanisms that turn mobile loops into stored dislocations, this new shear band mode consumes mobile dislocations that otherwise would contribute to the other storage mechanisms. The recovery rate of dislocations is assumed to be higher in the bands than elsewhere, and consequently it follows from the book-keeping of stored dislocations that a lower net increase of the total dislocation density is expected. The stage IV hardening, Eq. [8], related to the storage mode that decreases the subgrain size as explained above, will be less dominant if the shear bands consume a fraction of the dislocations.

If S_{IV} in Eq. [8] is assumed to be alloy-independent, the stage IV work-hardening rate will depend upon $\rho_i/\sqrt{\rho}$, which is observed to increase with solute concentration. If, however, this S_{IV} parameter is reduced to account for the shear banding that occurs, a lower θ_{IV} will be predicted. It is clearly seen from the low-temperature experiments by Sherby *et al.*[7] that the slope θ_{II} decreases as a function of increased Mg content. We have taken into account a similar decrease of $C = \alpha_1 G/\theta_{II}$ with increased Mg level to capture this (Figure 9(a)). Furthermore, it can be qualitatively concluded from micrographs that q_c increases with increased Mg solute level. Hence, C and q_c are mutually "balanced" in order to obtain the correct work-hardening rates in stage II, III, and early IV. Estimated values for these parameters as functions of the Mg content are applied in the model to

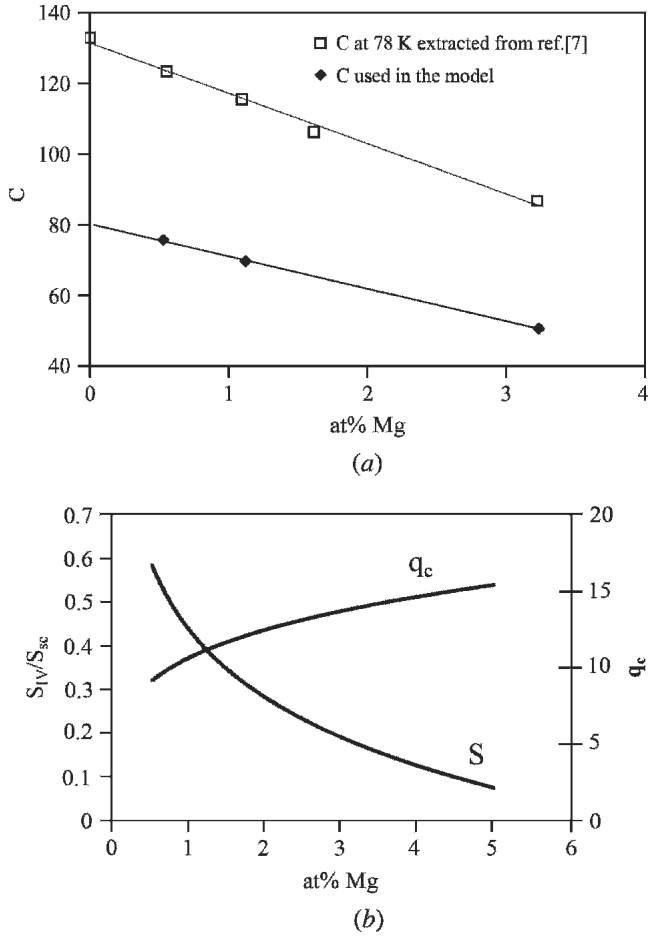

Fig. 9—(*a*) Variation in the C parameter as a function of at. pct Mg, extracted from data on binary AlMg alloys tested at 78K[7] and values used at room temperature in the work-hardening model. (*b*) Variation of S_{IV} and q_c with Mg content as used in the model calculations.

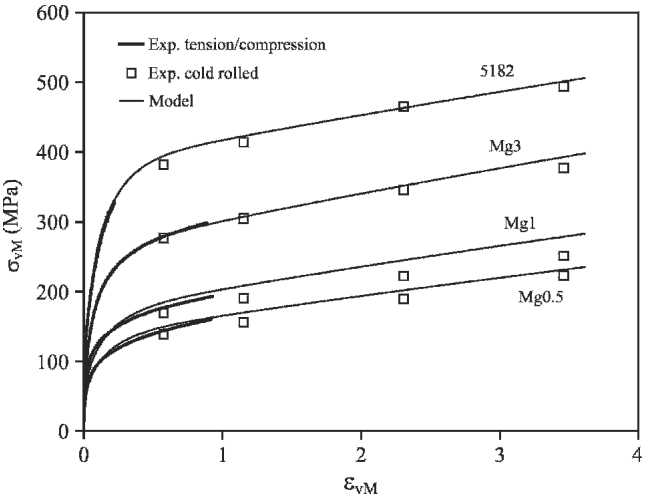

Fig. 10—Model predictions of the stress–strain behavior up to large strains for a range of AlMg alloys. Symbols indicate experimental data.

account for the storage pattern. The normalized parameter S_{IV}/S_{sc} is assumed to be 1 for a pure metal and decreases upon Mg addition (Figure 9(b)).

Figure 10 shows the modeled stress–strain curves up to large strains for the AlMgX alloys and AA5182. Experimental results from O-temper and cold-rolled materials are displayed for comparison, and it is seen that a reasonable agreement with the experimental stage IV results is obtained.

IV. CONCLUSIONS

In this work, the large strain work-hardening behavior is studied for a range of AlMg alloys. The stage IV work-hardening rate is shown to be almost independent of the solute content. The unexpectedly low work-hardening rate of high-Mg alloys is believed to result from an increased shear band formation, but also from a different storage pattern of dislocations in subgrain interior and boundaries. These effects are included in the model and give reasonable predictions for the work hardening in stage IV.

ACKNOWLEDGMENTS

This research was carried out as part of the EC Fifth Framework project VIRFORM, Contract No. G1RD-CT-1999-00155. Funding by the European Community and the industrial partners is gratefully acknowledged. Thanks also to Professor J.D. Embury for many interesting discussions.

REFERENCES

1. A.D. Rollett and U.F. Kocks: *Solid State Phenomena*, 1994, vol. 35–36, pp. 1-18.
2. G. Langford and M. Cohen: *Trans. Am. Soc. Metall.*, 1969, vol. 62, pp. 623-38.
3. J.M. Alberdi Garitaonandia: Ph.D. Thesis, University of Navarra, San Sebastian, 1984.
4. M. Zehetbauer and V. Seumer: *Acta Metall. Mater.*, 1993, vol. 41, pp. 577-88.
5. J.S. Hayes, R. Keyte, and P.B. Prangnell: *Mater. Sci. Technol.*, 2000, vol. 16, pp. 1259-63.
6. J. Gil Sevillano: in *Material Science and Technology. A Comprehensive Treatment*, R.W. Cahn (ed.), VCH, Weinheim, 1993, vol. 6, pp. 19-88.
7. O.D. Sherby, R.A. Anderson, and J.E. Dorn: *J. Metals*, 1951, pp. 643-52.
8. U.F. Kocks: *J. Eng. Mater. Technol.*, 1976, vol. 98, pp. 76-85.
9. U.F. Kocks and H. Mecking: *Prog. Mater. Sci.*, 2003, vol. 48, pp. 171-73.
10. P.S. Follansbee and U.F. Kocks: *Acta Metall.*, 1988, vol. 36, pp. 81-93.
11. A.D. Rollett, U.F. Kocks, and R.D. Doherty: in *Formability and Metallurgical Structure*, A.K. Sachdev and J.D. Embury (eds.), The Metallurgical Society, Orlando, 1987, pp. 211-25.
12. B. Holmedal, K. Martinsen, and E. Nes: in *Virtual Fabrication of Aluminum Alloys,* J. Hirsch (ed.), John Wiley & Sons, 2006.
13. F.B. Prinz and A.S. Argon: *Acta Metall.*, 1984, vol. 32, pp. 1021-28.
14. F. Roters, D. Raabe, and G. Gottstein: *Acta Mater.*, 2000, vol. 48, pp. 4181-89.
15. M. Zehetbauer: *Acta Metall. Mater.*, 1993, vol. 41, pp. 589-99.
16. F.R. Castro-Fernandez, C.M. Sellars, and J.A. Whiteman: *Mater. Sci. Technol.,* 1990, vol. 6, pp. 453-60.
17. A.S. Argon and P. Haasen: *Acta Metall. Mater.*, 1993, vol. 41, pp. 3289-306.
18. B. Holmedal, K. Marthinsen, and E. Nes: *Z. Metallk.*, 2005, vol. 96, pp. 532-45.
19. K. Marthinsen and E. Nes: *Mater. Sci. Technol.*, 2001, vol. 17, pp. 376-88.
20. E. Nes: *Prog. Mater. Sci.*, 1998, vol. 41, pp. 129-94.
21. E. Nes and K. Marthinsen: *Mater. Sci. Eng.*, 2002, vol. A322, pp. 176-93.
22. S. Zajac: Swedish Institute for Metals Research, Stockholm, Sweden, unpublished research, 1998.
23. B. Rønning: Hydro Aluminium Sunndal, Sunndalsøra, Norway, unpublished research, 1998.
24. O. Engler: Hydro Aluminium Deutschland, Bonn, Germany, unpublished research, 2002.
25. R.H. Wagoner and J.-L. Chenot: *Fundamentals of Metal Forming*, John Wiley & Sons, New York, 1996.
26. S. Li and P. Van Houtte: *Aluminium*, 2002, vol. 78, pp. 918-22.
27. P. Van Houtte: *The MTM-FHM Software System Manual*, Version 2, Katholieke Universiteit Leuven, Leuven, Belgium, 2000.
28. G.B. Burger, A.K. Gupta, P.W. Jeffrey, and D.J. Lloyd: *Mater. Charact.*, 1995, vol. 35, pp. 23-39.
29. Ø. Ryen, O. Nijs, E. Sjölander, B. Holmedal, H.E. Ebström, and E. Nes: *Metall. Trans. A*, 2006, vol. 37A, pp. 1999-2006.
30. V. Randle and O. Engler: *Introduction to Texture Analysis: Macrotexture, Microtexture and Orientation Mapping.* Gordon and Breach Science, Amsterdam, The Netherlands, 2000.
31. M. Koizumi, S. Kohara, and H. Inagaki: *Z. Metallk.*, 2000, vol. 91, pp. 88-96.
32. K. Lücke and O. Engler: *Mater. Sci. Technol.*, 1990, vol. 6, pp. 1113-30.
33. O. Engler, M. Crumbach, and S. Li: *Acta Mater.*, 2005, vol. 53, pp. 2241-57.
34. H. Inagaki and S. Kohara: *Z. Metallk.*, 1997, vol. 88, pp. 570-75.
35. A. Korbel, J.D. Embury, M. Hatherly, P.L. Martin, and H.W. Erbsloh: *Acta Metall.*, 1986, vol. 34, pp. 1999-2009.
36. H.J. Roven and E. Nes: *Metall. Sci.*, 1984, vol. 18, pp. 515-20.
37. S.V. Harren, H.E. Dève, and R.J. Asaro: *Acta Metall.*, 1988, vol. 36, pp. 2435-80.
38. H. Inagaki, M. Koizumi, C.S.T. Chang, and B.J. Duggan: in *Aluminium Alloys: Their Physical and Mechanical Properties*, P.J. Gregson and S.J. Harris (eds.), Trans Tech Publications, Switzerland, 2002, pp. 587-92.